Understanding and Control of Zener Pinning via Phase Field and Ensemble Learning

Sukriti Manna [*1,2], Henry Chan [†1,2], Avishek Ghosh[3],
Tamoghna Chakrabarti [‡4], and Subramanian Sankaranarayanan [§1,2]

[1]Center for Nanoscale Materials, Argonne National Laboratory,
Lemont, Illinois 60439, United States
[2]Department of Mechanical and Industrial Engineering, University of Illinois,
Chicago, Illinois 60607, United States
[3]Systems and Control Engg. and Centre for Machine Intelligence and Data Science,
Indian Institute of Technology Bombay, Mumbai 400076, India
[4]Department of Metallurgical & Materials Engineering,
Indian Institute of Technology Patna, Patna, 801106, India

July 14, 2023

Abstract

Zener pinning refers to the dispersion of fine particles which influences grain size distribution *via* movement of grain boundaries in a polycrystalline material. Grain size distribution in polycrystals has a significant impact on their properties including physical, chemical, mechanical, and optical to name a few. We explore the use of Phase-field modeling and machine-learning techniques to understand and improve the control of grain size distribution *via* Zener pinning in polycrystalline materials. We develop a machine learning model that determines the relative importance of various parameters to exercise microstructure control *via* Zener pinning. Our workflow combines high-throughput phase-field simulations and machine learning to address the computational bottlenecks associated with large-scale simulations as well as identify features necessary for microstructure control in polycrystals. A random forest (RF) regression model was developed to predict grain sizes based on five Phase-field model parameters, achieving an average prediction error of 0.72 nm for the training data and 1.44 nm for the test data. The importance of the input parameters is analyzed using the SHapley Additive exPlanations (SHAP) approach which reveals that diffusivity, volume fraction, and particle diameter are the most important parameters in determining the final grain size. These findings will allow us to select the best second-phase particles, optimize grain size distributions and thus design microstructures with the desired properties. The developed method is a highly versatile and generalizable approach that can be used to assess the combined effects of individual features in the presence of multiple variables.

1 Introduction

Grain size is a critical factor that significantly affects the mechanical, physical, and chemical properties of polycrystalline materials [1, 2, 3]. Controlling grain size is a vital aspect of material tailoring for specific applications. In metals, reducing grain size can increase their strength while maintaining ductility and toughness, making them a valuable material for aerospace and structural engineering [1]. Conversely, larger grain

[*]smanna@anl.gov
[†]hchan@anl.gov
[‡]tamoghna@iitp.ac.in
[§]skrssank@anl.gov

sizes are preferred for high-temperature applications due to their improved creep resistance [4]. Similarly, in ceramics, grain size strongly influences their optical, electrical, and magnetic properties, with smaller grain sizes improving transparency and larger grain sizes enhancing piezoelectric properties [5, 6, 7, 8, 9, 10, 11, 12].

Controlling the grain size of polycrystalline materials has been a subject of extensive research, and several techniques have been developed for this purpose. One widely used method is Zener Pinning, which was introduced by Smith and Zener and involves introducing second-phase particles to control grain size [13]. Despite its widespread use, the efficacy of this method is complex and dependent on several factors such as size, morphology, volume fraction, coherency, anisotropic interfacial energy, and coarsening of the second-phase particle [14]. The pinning effect exerted by second-phase particles on grain boundaries results in the limitation of grain boundary mobility and halts grain growth. The pinning pressure exerted by these particles, characterized by the particle size (P_d) and volume fraction (V_f), can be expressed as follows: $P_z = \frac{3V_f\gamma_{bd}}{2P_d}$. The particles' pinning pressure can prevent further grain growth once it equals the driving pressure, leading to the attainment of limiting grain size ($\overline{D_{lim}}$)[15].

$$\frac{\alpha\gamma_{bd}}{\overline{D_{lim}}} = \frac{3V_f\gamma_{bd}}{2P_d} \tag{1}$$

$$\overline{D_{lim}} = \frac{2P_d\alpha}{3V_f} \tag{2}$$

In a study conducted by Vanherpe et al. [16], it was demonstrated that the pinning effect of particles on grain boundaries increases with an increase in volume fraction and aspect ratio. The total fraction of particles present at the boundaries was higher with increasing volume fraction and aspect ratio, resulting in a higher pinning effect. An expression that relates the limiting grain size to the particle size, aspect ratio, and volume fraction is expressed below,

$$\overline{D_{lim}} = K\frac{l}{1+ar_a}\cdot\frac{1}{V_f^b} \tag{3}$$

Here, l is the long axis size of the particle, r_a is the aspect ratio and K, a and b are fitting parameters. The shape factor of second-phase particles is denoted by α in equation 3. The equation proposed by Zener, despite being widely used in practical applications to predict the limiting mean grain size, is considered simplistic and underestimates the pinning effect of the particle distribution. Furthermore, the analytical models discussed earlier have a significant limitation in that they require consideration of the characteristic dimple shape of a grain boundary near a grain boundary-particle interface, which poses a challenge in achieving a better understanding of the pinning effect. The complexity of estimating the pinning force exerted by a distribution of particles, given that only a fraction of the particles will be located at grain boundaries, also necessitates the use of simplifying assumptions.

This study aims to investigate the combined effects of multiple parameters on Zener pinning and improve its control by utilizing Phase-field modeling and machine-learning techniques. While analytical models have limitations in comprehending the pinning effect, Phase-field models have been used to analyze the impact of second-phase particle size, shape, and volume fraction on Zener pinning drag [17, 18, 19, 20]. However, a systematic investigation of the combined effects of these parameters has not been performed. As multiple parameters are often varied simultaneously in practical applications, a comprehensive examination of their combined effects is essential to improve Zener pinning control. To address this, Phase-field modeling is used to develop an ML model that determines the relative importance of various parameters, and a workflow (depicted in Figure 1) combining high-throughput Phase-field simulations and machine learning is introduced to explore the 5-dimensional parameter space and gain insights into Zener pinning. Our approach developed in this study is of general-purpose and can be applied to a wide range of materials phenomena influenced by multiple variables. Our workflow provides a comprehensive understanding of the combined effects of individual behaviors within diverse systems. This versatile methodology enables us to precisely tune individual parameters, allowing us to exert inverse control over the phenomenon. This capability can be leveraged to optimize and refine control strategies for enhanced outcomes.

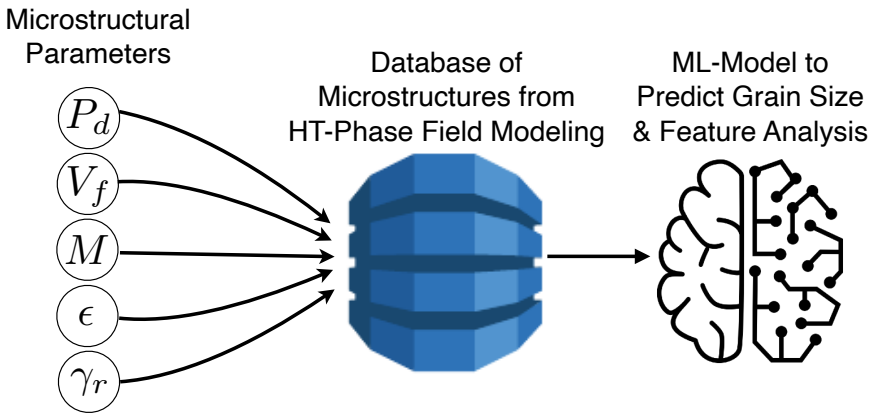

Figure 1: Our integrated methodology combining high-throughput Phase-field simulations and machine learning to explore Zener pinning in a 5-dimensional parameter space. The investigated microstructural parameters include initial precipitate diameter (P_d), volume fraction (V_f), diffusivity or mobility (M), shape defined by precipitate aspect ratio (ϵ), and the ratio of surface energy to grain boundary energy of the precipitates (γ_r).

2 Method

2.1 Theoretical Formulations for Phase-field Model

In this study, we investigate the microstructure of a Phase-field model, which consists of two distinct phases: the matrix and second-phase particles (or precipitates). The matrix is composed of multiple crystals or grains and is polycrystalline in nature, while the precipitates are single crystalline structures [21, 22]. Our main objective is to explore the effects of various properties of second-phase particles, including their morphology and physical properties, on grain growth in the matrix phase. Specifically, we aim to analyze how the size, shape, volume fraction, surface energy, and mobility of the precipitates influence grain growth in the matrix phase. Reference [23, 24] contains further information about the specifics of the Phase-field method.

2.1.1 Free Energy Functional

For our model system, the free energy functional F is given by,

$$F = N_v \int_{\Omega} [f(c, \eta_i) + \kappa_c (\nabla c)^2 + \sum_{i=1}^{n} \kappa_\eta (\nabla \eta_i)^2] d\Omega \tag{4}$$

where $f(c, \eta_i)$ is the bulk free energy per lattice site, κ_c and κ_η are the gradient energy coefficients for gradients in composition field c and order parameters η_i, respectively, $i = 1, 2, ..., n$ describes n unique grain orientations in the matrix phase. The bulk free energy density $f(c, \eta_i)$ is constructed in such a way that grains of the matrix phase and second particle phase are in equilibrium with each other across planar surfaces and grain boundaries. We have used the following form for $f(c, \eta_i)$:

$$f(c, \eta_i) = Ac^2(1-c)^2 + Bc^2\zeta(\eta_i) + Z(1-c)^2 \sum_{i=1}^{n} \eta_i^2 \tag{5}$$

$$\zeta(\eta_i) = \sum_{i=1}^{n} [\frac{\eta_i^4}{4} - \frac{\eta_i^2}{2} + 2 \sum_{j>i}^{n} \eta_i^2 \eta_j^2] + 0.25 \tag{6}$$

A, B, and Z are constants.

2.1.2 Kinetics of Microstructural Evolution

The temporal evolution of microstructure is governed by the Cahn-Hilliard equation [25] and the Allen-Cahn equation [26],

$$\frac{\partial c}{\partial t} = \nabla . M \nabla \mu \tag{7}$$

$$\frac{\partial \eta_i}{\partial t} = -L \frac{\delta (F/N_v)}{\delta \eta_i} \tag{8}$$

The mobility M is invariant of both the composition and the order parameter η, whereas N_V denotes the quantity of lattice sites within a given volume unit. The relaxation coefficient is represented by L.

Table 1: Simulation variables used in our high throughput Phase-field simulations

Model Parameters	Values
$\triangle x$	1.0
$\triangle y$	1.0
$\triangle t$	0.02
$N_x \times \triangle x$	512
$N_y \times \triangle y$	512
A	1.0
B	1.0
Z	1.0
κ_c	1.0
κ_η	1.0, 0.33
L	1.0
Micro-structural Parameters	**Values**
P_d	4.0-12.0
V_f	0.0-0.1
M	0.0-5.0
ϵ	0.25-1.0
$\gamma_{\text{surf}}/\gamma_{\text{gb}}$ or γ_r	1.0, 1.5

The kinetic equations are solved using the semi-implicit Fourier spectral method with periodic boundary conditions. The FFTW package is utilized for discrete Fourier transformations [27]. Details of the parameters utilized in the simulations can be found in Table 1. Our study focuses on the combined effect of five microstructural parameters, which are presented under the "Microstructural Parameters" sub-header in Table 1 along with their corresponding ranges of values. The surface-to-grain boundary energy ratio γ_r is varied by changing the κ_η as shown in Table 1 under the "Model Parameters" sub-header. We have selected two specific values (1 and 1.5) for the surface-to-grain boundary energy ratio in order to model hypothetical systems representing ceramic oxides and metallic materials, respectively. The rationale behind these choices is based on the relationship ($\gamma_{\text{gb}}/\gamma_{\text{surf}} = 2cos\frac{\phi}{2}$) between the grain boundary energy-to-surface energy ratio ($\gamma_{\text{gb}}/\gamma_{\text{surf}}$) and the dihedral angle (ϕ). In ceramic oxide systems, the dihedral angle is typically around 120°, resulting in a ratio close to 1. On the other hand, in many metallic systems, the ratio is often 2 or higher [28]. Therefore, by considering these factors, we have opted for the values of 1 or 1.5 to accurately represent the respective systems in our study. Also, we have not accounted for misorientation effects on grain boundary energy, by assuming isotropy *i.e.* the energy is independent of grain misorientation. To calculate the area of both matrix grains and second-phase particles, the Hoshen-Kopelman algorithm [29] is employed.

2.1.3 Nondimensionalization

The non-dimensionalization has been carried out based on the following relationships:

$$E^{'} = A^{'} \tag{9}$$

$$L^{'} = \left(\frac{\kappa_c^{'}}{A^{'}}\right)^{\frac{1}{2}} \tag{10}$$

$$T^{'} = \frac{(c_p^{'} - c_m^{'})^2 L^{'2}}{M^{'} E^{'}} \tag{11}$$

$$M^{'} = \frac{(c_p^{'} - c_m^{'})^2 D^{'}}{2A^{'}} \tag{12}$$

Table 2 presents the non-dimensional parameters used in our model, which have been obtained through the non-dimensionalization of variables using the characteristic length L', energy E', and time T'. The prime symbol represents dimensional quantities, while unprimed quantities indicate non-dimensional variables in the formulation. Dimensional values of non-dimensionalized parameters are shown in Table 2.

Table 2: Dimensional values of non-dimensionalized parameters

Parameters	Values
Characteristics Length $L^{'}$	1.0 nm
Characteristics Energy $E^{'}$	4.8×10^{-21} J
Characteristics Time $T^{'}$	2.1×10^{-4} sec
Interfacial Energy $\gamma^{'}$	0.1 J/m^2
Diffusivity$D^{'}$	1×10^{-14} m^2/sec
Mobility($M^{'}$)	1.04×10^{6} m^2/J-sec

2.2 Machine Learning Model

Here, we chose to build a random forest (RF) regression model [30] for learning the relationships between final grain size and the 5 Phase-field model parameters, namely diameter (P_d), volume fraction (V_f), aspect ratio (ϵ) of the pinning particles, as well as diffusivity (M) and surface-to-grain-boundary energy ratio (γ_r). Our RF model consists of a collection of decision trees trained using a bootstrapping process, which leverages a bagging technique (i.e., ensemble learning) to reduce the variance in the grain size predictions. A grid search approach is used to explore different combinations of RF model hyper-parameters, such as the number of trees (1, 2, 4, 8, 16, 32, 64, 128, 256, 512, 1024, 2048, 4096), splitting criterion (absolute error), maximum tree depth (3, 4, 5, 6, 7, 8, 9, unlimited), and the number of leaf nodes (unlimited). The optimal hyper-parameters are found to be 128 trees with an unlimited number of leaf nodes, a maximum tree depth of 7, no pruning, and one randomly selected feature at each node splitting.

3 Results and Discussions

3.1 The evolution of microstructures from Phase-field simulations

In this study, we used high-throughput Phase-field modeling to investigate the impact of various parameters on grain coarsening. Our Phase-field model allowed us to explore the effects of particle shape as defined by its aspect ratio (ϵ), particle volume fraction (V_f), particle size (P_d), mobility (M), and surface-to-grain boundary energy ratio (γ_r) on grain growth in a polycrystalline matrix phase. The parametric values were non-dimensionalized and presented in Table 1. To analyze the microstructures of grain coarsening in the presence of second-phase precipitates, we considered representative simulated microstructures, as shown in Figure 2(a)-(f). Furthermore, we plotted the corresponding grain size versus the time plot, as shown in Figure 3. The results demonstrate that grain boundaries reach a limiting size at the end of the simulation in most cases, which is consistent with Equation 2. We performed simulations over a wide range

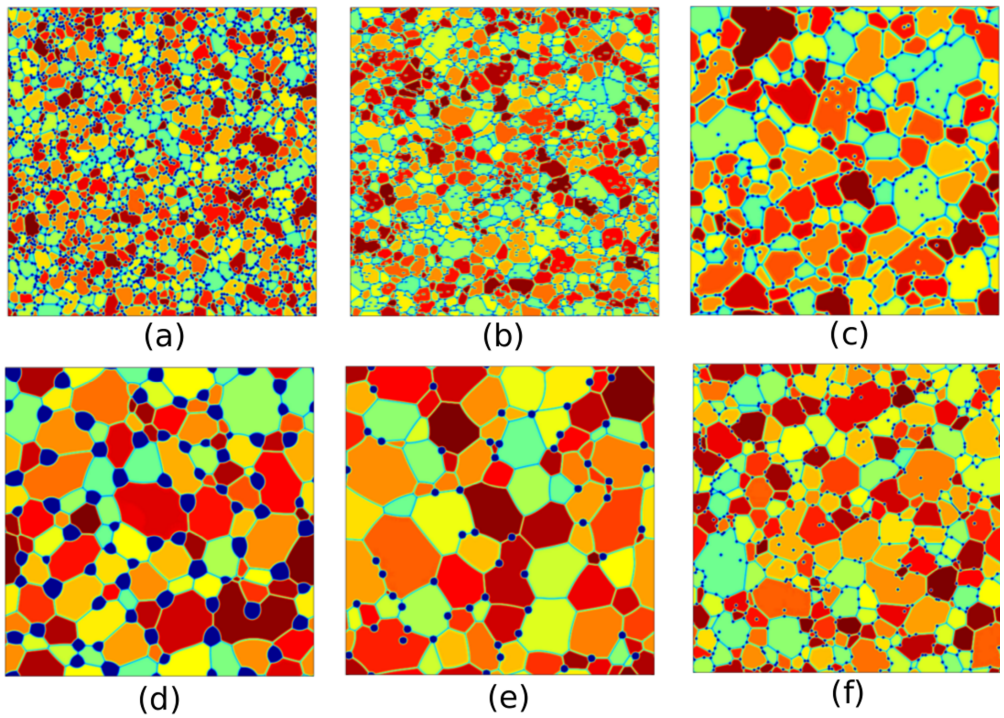

Figure 2: The impact of different factors on Zener pinning is investigated using Phase-field modeling. Panel (a) shows a small-sized spherical particle with a large volume fraction of 0.1, which results in a more significant pinning effect. Panel (b) depicts a small particle with a low volume fraction of 0.025 and a high aspect ratio (ϵ), which results in an elongated grain shape due to the preferred growth direction parallel to the particle's long axis. Panel (c) shows a small-sized spherical particle with a low volume fraction of 0.025 and a lower surface-to-grain boundary energy ratio, which results in a reduced pinning effect. In panel (d), a small-sized particle with a low volume fraction of 0.025 and a high mobility of 1.0 is depicted, resulting in reduced pinning and increased grain growth. Panel (e) displays a large-sized spherical particle (12 nm) with a low volume fraction of 0.025, which exhibits a weak pinning effect. Lastly, panel (f) illustrates a small-sized spherical particle (4 nm) with a low volume fraction of 0.025, resulting in a weak pinning effect and a near-uniform grain size distribution.

of particle sizes, volume fractions, aspect ratios, mobility, and interface-to-grain boundary energy ratios, and all microstructures were analyzed at a later stage (t = 15000). Our findings provide insights into the effect of various parameters on grain coarsening and offer a useful reference for future studies in this field.

Our findings indicate that particle size (P_d) and mobility (M) negatively affect the Zener pinning, as larger particle sizes and higher mobilities result in lower pinning effects, while particle volume fraction (V_f) and surface-to-grain boundary energy ratio ($\frac{\gamma_{surf}}{\gamma_{gb}}or\gamma_r$) positively affect the pinning, as increasing them enhances the pinning effect, as shown in Figure 2(e)-(f) and Figure 2 (a)-(c). Moreover, we found that the aspect ratio (ϵ) also influences the Zener pinning, as shown in Figure 2 (b)-(f), with a lower aspect ratio showing a better pinning effect. These results are consistent with the Zener pinning equation (Equation 2) and previous studies, such as the work by K. Chang *et al* [31], which found that smaller particle sizes and needle-shaped particles are more effective in pinning grain boundaries for the same volume fraction. Overall, our Phase-field modeling provides insights into the effect of various parameters on Zener pinning, which can guide the design and optimization of materials with desired microstructural properties.

3.2 Machine Learning model for grain size prediction

To quickly predict grain size, we use a machine learning regression model to model the outcomes of our high-throughput Phase-field simulations, as the impact of various input parameters on the final grain size

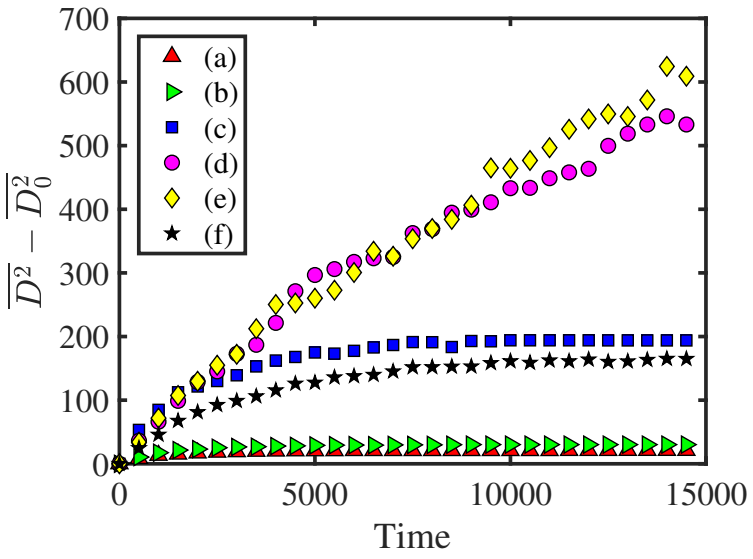

Figure 3: This plot shows the grain size evolution over time for the simulated microstructures depicted in Figure 2 (a)-(f), where $\bar{D}$ is instantaneous average grain size and $\bar{D}_0$ is the initial average grain size. The data points represent the average grain size in the microstructure at each time step. As shown in the plot, all microstructures exhibit an initial stage of rapid grain growth, followed by a slower growth stage, until a limiting grain size is reached at the end of the simulation time ($t = 15000$). It is interesting to note that the microstructures with higher volume fractions and higher surface-to-grain boundary energy ratio exhibit slower grain growth and reach a smaller limiting grain size, indicating a stronger Zener pinning effect. Conversely, microstructures with larger particle sizes, lower particle volume fractions, and lower surface-to-grain boundary energy ratios exhibit faster grain growth and reach a larger limiting grain size, indicating weaker Zener pinning. The effect of particle aspect ratio and mobility on grain growth is also evident in the plot, with smaller aspect ratios and higher mobilities leading to faster grain growth and larger limiting grain size. These results are consistent with the observations made from the microstructure analysis and further, confirm the importance of the investigated parameters in controlling grain growth and Zener pinning in the presence of second-phase precipitates.

is intricate and non-linear. A total of ~ 198 data points are obtained from the high-throughput Phase-field simulations. A multivariate visualization of the data is shown in Figure 4a. We randomly shuffled and split the data into 179 training data points and 19 test data points (*i.e.*, $\sim 10\%$ split). The training data is used to train the RF model and the test data, which is not seen by the model during the training procedure, is used to validate the model performance. All data points are weighted equally. The best model is selected based on averaged prediction errors from repeated (1000 times) training and validation of the model. The average grain size prediction error of our best RF model is around 0.72 nm for the training data and 1.44 nm for the test data. The parity plot in Figure 4b shows that the model performs well for grain sizes ranging from ~ 5 nm to ~ 40 nm.

The trained RF model can be used for fast and accurate prediction of grain sizes for a given set of Phase-field simulation input parameters. To explain its good performance, we analyzed it using the SHapley Additive exPlanations (SHAP) approach [32]. SHAP employs the classic Shapley values from game theory to quantify the contributions of individual features to the output of a ML model. In our case, it quantifies the importance of the 5 Phase-field simulation input parameters in our grain size prediction model. Figure 4c summarizes the SHAP results. The beeswarm plot at the top shows the SHAP values of all data points for the 5 features (simulation input parameters) and is colored by the feature values. Diffusivity is found to be the most important feature followed by volume fraction (V_f), aspect ratio (ϵ), particle diameter (P_d), and surface-to-grain-boundary energy ratio (γ_r) is found to be the least important feature. Larger values of diffusivity, aspect ratio, and particle diameter lead to larger predicted grain sizes, whereas larger values of particle volume fraction and surface-to-grain-boundary energy ratio lead to smaller predicted grain sizes.

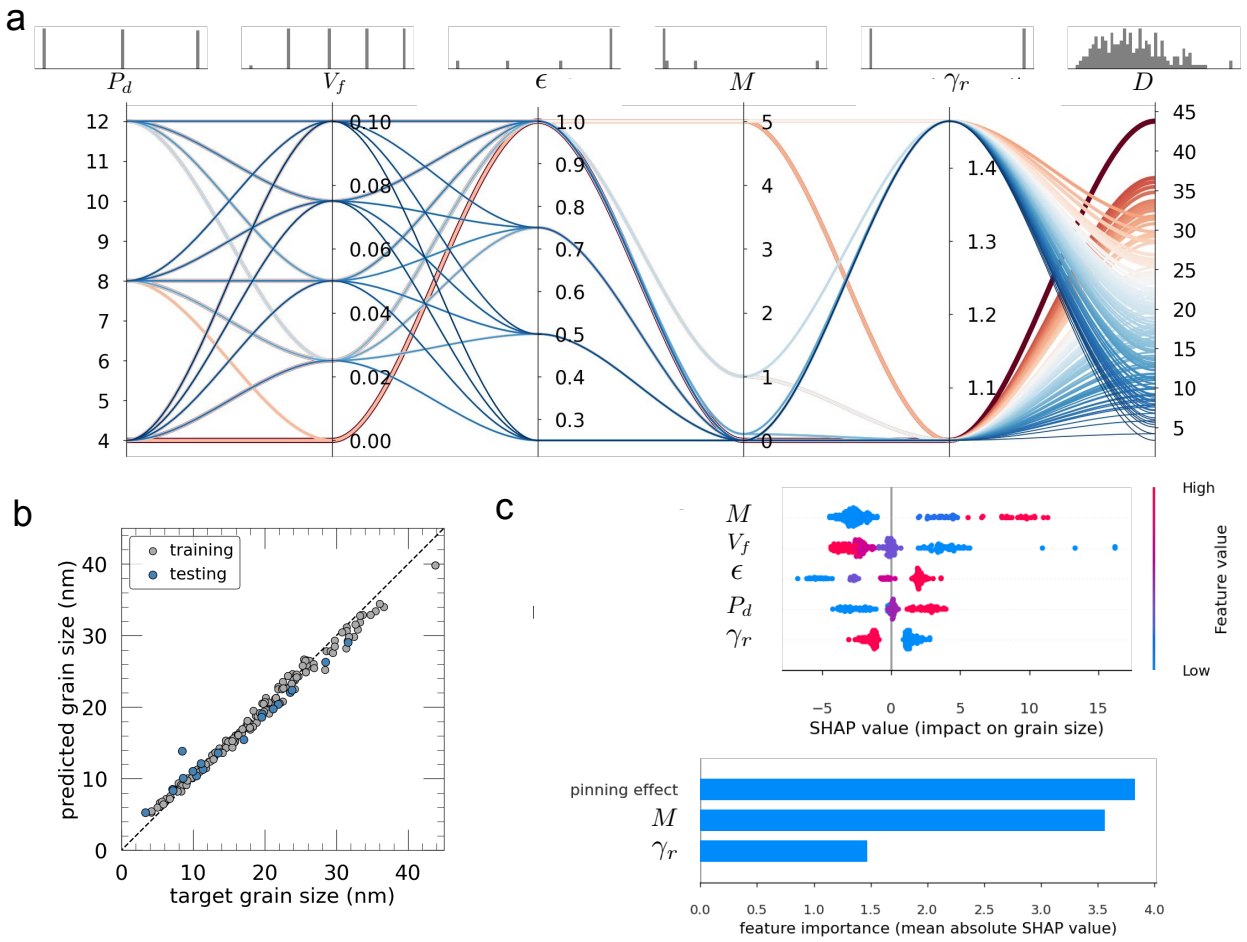

Figure 4: Multivariate visualization of Phase-field simulation data and grain size prediction using a random forest regression model. (a) Normalized distributions and a parallel coordinate plot of the 5 Phase-field input parameters: initial precipitate diameter (P_d), volume fraction (V_f), diffusivity or mobility (M), shape defined by precipitate aspect ratio (ϵ), and the ratio of surface energy to grain boundary energy of the precipitates (γ_r) and the final grain size (D) obtained from the simulations. The parallel coordinate plot visualizes the relationship across input parameters and the observed grain sizes. Each line represents a data point, which corresponds to a Phase-field simulation run. To help resolve overlapping, the lines are colored and with thicknesses set proportional to the grain sizes. (b) Parity plot showing the accuracy of grain size predictions of both the training and testing datasets by our random forest model. (c) Beeswarm and bar plots showing the Shapley values of the features (*i.e.*, simulation input parameters) for explaining their impact on the grain size predicted by our trained model. The features are ranked from top to bottom based on their importance. The pinning effect combines the contributions from the volume fraction (V_f), initial precipitate diameter (P_d), and aspect ratio (ϵ) of the pinning particles.

The bar plot at the bottom of Figure 4c shows that the pinning effect, which is the combined contribution of volume fraction, aspect ratio, and diameter of the pinning particle, is about equal or slightly more important than diffusivity in determining the predicted final grain size.

4 Summary and Conclusions

The integration of high throughput Phase-Field modeling and machine-learning techniques has been demonstrated as a successful approach for understanding and improving the control of Zener pinning in this study. The resulting random forest regression model can predict grain sizes based on five Phase-field model parameters. The model's performance was evaluated using both training and test datasets, achieving high accuracy with an average prediction error of 0.72 nm and 1.44 nm, respectively. The SHapley Additive exPlanations (SHAP) approach was used to determine the relative importance of each parameter, providing critical insights into the underlying mechanisms of Zener pinning. The findings reveal that diffusivity, volume fraction, and particle diameter are the most important parameters in determining the final grain size. This understanding will enable us to select appropriate second-phase particles to optimize final grain size and design materials with desired mechanical properties.

Our workflow provides a surrogate ML model that addresses the computational expense of phase-field simulations, enabling a more efficient and effective approach to extract key features and explore the impact of various parameters on Zener pinning. The results of this study have significant implications for improving material properties and advancing materials engineering. This approach can be extended to other materials systems and will enable us to develop a fundamental understanding of the role of various parameters in Zener pinning. By gaining a better understanding of the underlying mechanisms of grain coarsening and Zener pinning, we can design materials with desired grain structures and mechanical properties.

5 Acknowledgment

We acknowledge funding from BES Award DE-SC0020201 by DOE to support this research. The use of the Center for Nanoscale Materials, an Office of Science user facility, was supported by the U.S. Department of Energy, Office of Science, Office of Basic Energy Sciences, under Contract No. DE-AC02-06CH11357. This research used resources of the National Energy Research Scientific Computing Center, which was supported by the Office of Science of the U.S. Department of Energy under Contract No. DE-AC02-05CH11231. An award of computer time was provided by the Innovative and Novel Computational Impact on Theory and Experiment (INCITE) program of the Argonne Leadership Computing Facility at the Argonne National Laboratory, which was supported by the Office of Science of the U.S. Department of Energy under Contract No. DE-AC02-06CH11357. SKRS acknowledges UIC start-up funds for supporting this research. The author TC would like to thank DST for the financial support through Inspire Faculty Award (DST/INSPIRE/04 /2017/000548) and also IIT Patna for the facilities.

6 Data availability

The raw data can be accessed via the DOI: http://doi.org/10.5281/zenodo.8123162.

References

[1] Ning Wang, Zhirui Wang, KT Aust, and Uwe Erb. Effect of grain size on mechanical properties of nanocrystalline materials. *Acta Metallurgica et Materialia*, 43(2):519–528, 1995.

[2] V Metan and K Eigenfeld. Controlling mechanical and physical properties of al-si alloys by controlling grain size through grain refinement and electromagnetic stirring. *The European Physical Journal Special Topics*, 220(1):139–150, 2013.

[3] S Sulaiman, S Izman, MB Uday, and MF Omar. Review on grain size effects on thermal conductivity in zno thermoelectric materials. *RSC advances*, 12(9):5428–5438, 2022.

[4] B Wilshire and CJ Palmer. Grain size effects during creep of copper. *Scripta materialia*, 46(7):483–488, 2002.

[5] M Stefanski, L Marciniak, D Hreniak, and W Strek. Influence of grain size on optical properties of sr2ceo4 nanocrystals. *The Journal of chemical physics*, 142(18):184701, 2015.

[6] MJ Sablik. Modeling the effect of grain size and dislocation density on hysteretic magnetic properties in steels. *Journal of Applied Physics*, 89(10):5610–5613, 2001.

[7] Sukriti Manna, Mingyuan Wang, Adrian Barbu, and Cristian V Ciobanu. Machine-learning of piezoelectric coefficients for wurtzite crystals. *Materials and Manufacturing Processes*, pages 1–12, 2023.

[8] Ce-Wen Nan, A Tschöpe, S Holten, H Kliem, and R Birringer. Grain size-dependent electrical properties of nanocrystalline zno. *Journal of applied physics*, 85(11):7735–7740, 1999.

[9] Yachao Chen, Sukriti Manna, Cristian V Ciobanu, and Ivar E Reimanis. Thermal regimes of li-ion conductivity in β-eucryptite. *Journal of the American Ceramic Society*, 101(1):347–355, 2018.

[10] Yachao Chen, Sukriti Manna, Badri Narayanan, Zhongwu Wang, Ivar E Reimanis, and Cristian V Ciobanu. Pressure-induced phase transformation in β-eucryptite: An x-ray diffraction and density functional theory study. *Scripta Materialia*, 122:64–67, 2016.

[11] Sukriti Manna. *Design and discovery of new piezoelectric materials using density functional theory*. Colorado School of Mines, 2018.

[12] Kiyoshi Okazaki and Kunihiro Nagata. Effects of grain size and porosity on electrical and optical properties of plzt ceramics. *Journal of the American Ceramic Society*, 56(2):82–86, 1973.

[13] Cyril Stanley Smith. Grains, phases, and interfaces: An introduction of microstructure. *Trans. Metall. Soc. AIME*, 175:15–51, 1948.

[14] Tamoghna Chakrabarti and Sukriti Manna. Zener pinning through coherent precipitate: A phase-field study. *Computational Materials Science*, 154:84–90, 2018.

[15] Manohar PA, M Ferry, and T Chandra. Five decades of the zener equation. *ISIJ international*, 38(9):913–924, 1998.

[16] Liesbeth Vanherpe, Nele Moelans, Bart Blanpain, and Stefan Vandewalle. Pinning effect of spheroid second-phase particles on grain growth studied by three-dimensional phase-field simulations. *Computational Materials Science*, 49(2):340–350, 2010.

[17] Yoshihiro Suwa, Yoshiyuki Saito, and Hidehiro Onodera. Phase field simulation of grain growth in three dimensional system containing finely dispersed second-phase particles. *Scripta Materialia*, 55(4):407–410, 2006.

[18] Stefan Othmar Poulsen, PW Voorhees, and Erik Mejdal Lauridsen. Three-dimensional simulations of microstructural evolution in polycrystalline dual-phase materials with constant volume fractions. *Acta Materialia*, 61(4):1220–1228, 2013.

[19] Yongbiao Wang, Liming Peng, Yujuan Wu, Yan Zhao, Yongxin Wang, Yongbing Huang, and Wenjiang Ding. Phase-field modeling the effect of misfit on the precipitation of the second-phase particles and grain coarsening. *Computational Materials Science*, 100:166–172, 2015.

[20] Nele Moelans, Bart Blanpain, and Patrick Wollants. Phase field simulations of grain growth in two-dimensional systems containing finely dispersed second-phase particles. *Acta Materialia*, 54(4):1175–1184, 2006.

[21] Long-Qing Chen. Phase-field models for microstructure evolution. *Annual Review of Materials Research*, 32(1):113–140, 2002.

[22] Danan Fan, Long-Qing Chen, SP Chen, and Peter W Voorhees. Phase field formulations for modeling the ostwald ripening in two-phase systems. *Computational Materials Science*, 9(3):329–336, 1998.

[23] Tamoghna Chakrabarti, Nisha Verma, and Sukriti Manna. Grain boundary driven plateau–rayleigh instability in multilayer nanocrystalline thin film: A phase-field study. *Materials & Design*, 119:425–436, 2017.

[24] Tamoghna Chakrabarti and Rajdip Mukherjee. Effect of heterogeneous particle size on nanostructure evolution: A phase-field study. *Computational Materials Science*, 169:109115, 2019.

[25] John W Cahn. On spinodal decomposition. *Acta metallurgica*, 9(9):795–801, 1961.

[26] Samuel Miller Allen and John W Cahn. Ground state structures in ordered binary alloys with second neighbor interactions. *Acta Metallurgica*, 20(3):423–433, 1972.

[27] Matteo Frigo and Steven G Johnson. The design and implementation of fftw3. *Proceedings of the IEEE*, 93(2):216–231, 2005.

[28] Michel Barsoum. *Fundamentals of ceramics*. CRC press, 2019.

[29] Joseph Hoshen and Raoul Kopelman. Percolation and cluster distribution. i. cluster multiple labeling technique and critical concentration algorithm. *Physical Review B*, 14(8):3438, 1976.

[30] Tin Kam Ho. Random decision forests. In *Proceedings of 3rd international conference on document analysis and recognition*, volume 1, pages 278–282. IEEE, 1995.

[31] Kunok Chang, Weiming Feng, and Long-Qing Chen. Effect of second-phase particle morphology on grain growth kinetics. *Acta Materialia*, 57(17):5229–5236, 2009.

[32] Scott M Lundberg and Su-In Lee. A unified approach to interpreting model predictions. *Advances in neural information processing systems*, 30, 2017.